Measurement-Based Real-Time Voltage Stability Monitoring for Load Areas

Fengkai Hu, *Student Member, IEEE*, Kai Sun, *Senior Member, IEEE*, Alberto Del Rosso, *Member, IEEE*, Evangelos Farantatos, *Member, IEEE*, Navin Bhatt, *Fellow, IEEE*

***Abstract*--This paper proposes a measurement-based voltage stability monitoring method for a load area fed by *N* tie lines. Compared to a traditional Thevenin equivalent based method, the new method adopts an *N*+1 buses equivalent system so as to model and monitor individual tie lines. For each tie line, the method solves the power transfer limit against voltage instability analytically as a function of all parameters of that equivalent, which are online identified from real-time synchronized measurements on boundary buses of the load area. Thus, this new method can directly calculate the real-time power transfer limit on each tie line. The method is first compared with a Thevenin equivalent based method using a four-bus test system and then demonstrated by case studies on the NPCC (Northeast Power Coordinating Council) 48-machine, 140-bus power system.**

***Index Terms*--Load center, *N*+1 buses equivalent, parameter estimation, PMU, power transfer limit, Thevenin equivalent, voltage stability margin.**

I. Introduction

GROWTHS in electrical energy consumptions and penetration of intermittent renewable resources would make power transmission systems more often operate close to their stability limits. Among all stability issues, voltage instability due to the inability of the transmission or generation system to deliver the power requested by loads is one of major concerns in today's power system operations [1]. Usually, voltage instability initiates from a local bus but may develop to wide-area or even system-wide instability. At present, some electricity utilities use model-based online Voltage Stability Assessment (VSA) software tools to assist operators in foreseeing potential voltage instability. Based on a state estimate on the operating condition, those software tools employ power system models to simulate assumed disturbances such as contingencies and load changes. However, such a model-based approach has its limitations: the fidelity of its results highly depends on the accuracy of power system models; it needs a convergent, accurate state estimate in order to conduct stability assessment, which may be hard to obtain under stressed system conditions.

Many countries are deploying synchronized phasor measurement units (PMUs) on transmission systems to provide wide-area measurements for real-time stability monitoring. That leads to more interests in developing measurement-based VSA methods to directly assess voltage stability from measurements on monitored buses [2]-[23]. A family of measurement-based methods is based on Thevenin's Theorem: local measurements at the monitored load bus or area are used to estimate a Thevenin equivalent (TE) approximating the rest of the system, i.e. a voltage source connected through a Thevenin impedance; the power transfer to the monitored load reaches its maximum when that Thevenin impedance has the same magnitude as the load impedance [4], [5]. Based on a TE, voltage stability indices can be obtained [6], [7]. Multiple such equivalents may together be applied to a load area [8]. For practical applications, paper [9] demonstrates a TE-based method on realistic EHV network, and some other works consider load tap changers and over-excitation limiters in their models for better detection of voltage instability [10]-[12]. Influences from system-side changes and measurement errors on TE estimation are concerned in [13]. The equivalent circuit considering HVDC integrated wind energy is studied in [14].

Basically, a TE-based method works satisfactorily on a radially-fed load bus or a transmission corridor, and its computational simplicity makes it suitable for real-time application. In recent years, some research efforts have been on how to extend the application of the TE to a broader transmission system, e.g., the coupled single-port circuit or the Channel Components Transform [15]-[19]. Some other efforts tested TE-based methods on load areas. References [20] and [21] apply a TE-based method to a load center area. The method requires synchronized measurements on all boundary buses of the area in order to merge them into one fictitious load bus, for which a TE can be estimated and applied. That method was demonstrated on a real power transmission system in the real-time environment using PMU data [22]. Paper [23] improves the TE estimation for a load area to tolerate better the fluctuations in voltage phase angles and power factors measured at boundary buses. Paper [24] proposes a measurement- and model-based hybrid approach using the TE to assess voltage stability under N-1 contingencies.

However, as illustrated in [25], a TE-based method may not provide accurate voltage stability margin for each of multiple tie lines together feeding a load area if it merges those tie lines as done in [20] and [21]. Even when estimating the total transfer limit of multiple tie lines, the TE is accurate only if the boundary buses through which those tie lines feed the load area are strongly connected and the external system is coher-

This work is supported by the Electric Power Research Institute and the US Department of Energy (under award DE-OE0000628).

F. Hu and K. Sun are with the Department of Electrical Engineering and Computer Science, University of Tennessee, Knoxville, TN, USA (e-mail: fhu1@vols.utk.edu; kaisun@utk.edu). A. Del Rosso, E. Farantatos, and N. Bhatt are with the Electric Power Research Institute, Knoxville, TN, USA (email: adelrosso@epri.com; efarantatos@epri.com; nbhatt@epri.com).

ent so as to be regarded as a single voltage source. Those are two necessary conditions for merging tie lines and boundary buses and developing a meaningful TE. If connections between boundary buses are weak, when the load of the area gradually increases, tie lines may reach their power transfer limits at different time instants. In other words, voltage instability may initiate near one of boundary buses and then propagate to the rest of the area. Thus, only monitoring the total power transfer limit of all tie lines using a single TE may delay the detection of voltage instability.

This paper will extend and generalize the TE-based approach for voltage stability monitoring to a unified approach based on the identification of an *N*+1 buses equivalent system. This new equivalent has *N* buses interconnected to represent a load area with *N* boundary buses and one voltage source representing the external system. In fact, the TE is its special case with *N*=1. By modeling boundary buses separately for a load area, a new method based on that equivalent is developed and demonstrated in this paper to calculate power transfer limits at individual boundary buses.

In the rest of the paper, section II introduces the new method in detail, including the *N*+1 buses equivalent system, its parameter identification and analytical solutions of power transfer limits of its tie lines. In section III, an online scheme to implement the new method is presented. Section IV first uses a four-bus power system to illustrate the advantages of the new method over a traditional TE-based method, and then validates the new method on the NPCC 48-machine, 140-bus power system. Finally, conclusions are drawn in section V.

II. Proposed *N*+1 Buses Equivalent System

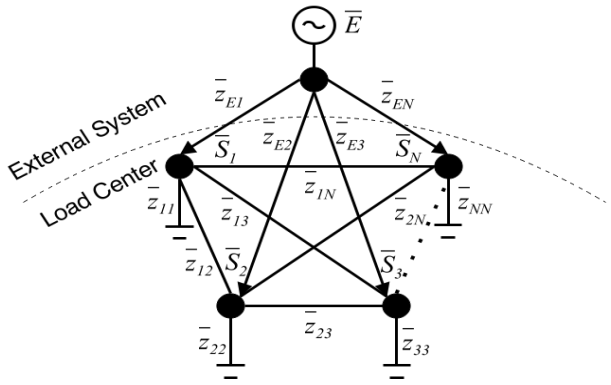

Fig. 1. *N*+1 buses equivalent.

For a load area fed by *N* tie lines, voltage instability may be a concern with its boundary buses when power flows of those tie lines approach to their transfer limits. As shown in Fig. 1, an *N*+1 buses equivalent system is proposed to model those boundary buses and tie lines while reducing the network details both inside and outside of the load area. Assume the external system to be strongly coherent without any angular stability concern. Thus, it is represented by a single voltage source with phasor $\bar{E}$ connected by *N* branches with impedances $\bar{z}_{E1} \sim \bar{z}_{EN}$ (representing *N* tie lines) to *N* boundary buses, respectively. Each boundary bus is monitored and connects an equivalent load with impedance $\bar{z}_{ii}$ modeling the portion of load seen from that bus. Connection between any two boundary buses *i* and *j* is modeled by impedance $\bar{z}_{ij}$. The power transfer limit of each tie line is a function of $N(N-1)/2+2N+1$ complex parameters of that equivalent system including voltage phasor $\bar{E}$, *N* tie-line impedances $\bar{z}_{Ei}$'s, $N(N-1)/2$ transfer impedances $\bar{z}_{ij}$'s and *N* load impedances $\bar{z}_{ii}$'s.

Let $\bar{S}_i = P_i + jQ_i$ denote the complex power fed to boundary bus *i* and let $\bar{V}_i$ denote the bus voltage phasor. Using synchronized measurements on $\bar{S}_i$ and $\bar{V}_i$, all parameters of the equivalent can be identified online (e.g. every 0.1~1s) using the latest measurements of a sliding time window. The rest of the section presents the algorithms for estimating the parameters of the external system (i.e. $\bar{E}$ and $\bar{z}_{Ei}$) and the load area (i.e. $\bar{z}_{ii}$ and $\bar{z}_{ij}$) and then derives the analytical solution of each tie-line power transfer limit.

A. Identification of External System Parameters

Assume that the sliding time window contains *K* measurement points. The external system parameters are assumed to be constant during the time window and hence are estimated by solving the following optimization problem. Nodal power injection equation (1) holds at each measurement point *k* of the time window.

$$\bar{S}_i(k) = \left(\frac{\bar{E} - \bar{V}_i(k)}{\bar{z}_{Ei}}\right)^* \times \bar{V}_i(k) \qquad k=1\sim K \tag{1}$$

where $\bar{S}_i(k) = P_i(k) + jQ_i(k)$ and $\bar{V}_i(k) = V_i(k)\angle\theta_i(k)$ are respectively the received complex power and voltage phasor at boundary bus *i* at time point *k*. The magnitude of $\bar{E}$, denoted by *E*, can be estimated from measurements at each boundary bus *i*, whose estimation error is

$$e_i^{ex}(k) = E - \left|(P_i(k) - jQ_i(k))(r_{Ei} + jx_{Ei}) + (V_i(k))^2\right| / V_i(k) \tag{2}$$

The optimization problem in (3) computes the optimal estimates of *E*, r_{Ei} and x_{Ei}.

$$\min J^{ex} = \sum_{k=1}^{K}\sum_{i=1}^{N}\frac{\omega_e}{N}\left[e_i^{ex}(k)\right]^2 + \sum_{i=1}^{N}\omega_z\left(\frac{r_{Ei}}{r_{Ep}} - 1\right)^2 + \sum_{i=1}^{N}\omega_z\left(\frac{x_{Ei}}{x_{Ep}} - 1\right)^2$$
$$s.t. \quad E > 0, \quad r_{Ei} \geq 0 \tag{3}$$

The 1st term summates the estimation errors of *E* for all buses and all time points. The 2nd and 3rd terms respectively summate normalized differences in r_{Ei} and x_{Ei} between the estimates for the current and previous time window. ω_e and ω_z are weighting factors respectively for variances of *E* and $\bar{z}_{Ei}$ over the time window. For instance, if the network topology of the external system does not change, $\bar{z}_{Ei}$ will be constant. Thus, there should be $\omega_z > \omega_e$ to allow more changes in *E*. The Sequential Quadratic Programming (SQP) method is used to solve the optimization problem in (3) [26].

The above optimization problem for the external system is actually a non-convex problem, so it needs to select good initial values for the external system parameters. As long as the initial values are in a neighborhood of the optimum that is considered as the true solution, the SQP method can make sure

to converge to that solution. However, the problem does have multiple local optima. In practice, the initial values of external system parameters for optimization are determined as follows: at the beginning when the new measurement-based method is performed or whenever a major disturbance, e.g. a line outage and a generator outage, is detected on the external system, the Least Square method is applied to the *K* data points of the current time window to estimate the parameters as new initial values; otherwise, the new method selects initial values from the optimization results of the previous time window. Because of the non-convex nature of this optimization problem, if the initial values selected at the beginning are far from the true solution, the optimization may converge to a different solution with errors in parameter estimation and consequently cause inaccurate transfer limits at the end. Those errors may last until the next time the Least Square method is performed to re-create new initial values. Later in a case study on the NPCC system, the results from different initial values with errors intentionally added are compared. In practice, the Least Square method may be performed at a certain frequency, e.g. every a few minutes, even if a major disturbance is not detected.

B. Identification of Load Area Parameters

Load area parameters include load impedance $\bar{z}_{ii}$ and transfer impedance $\bar{z}_{ij}$ (*i* and *j*=1~*N*), whose admittances are $\bar{y}_{ii}$ and $\bar{y}_{ij}$. In each time window, assume constant $\bar{y}_{ij}$ if there is no topology change in the load area, and allow $\bar{y}_{ii}$ to change. From power flow equations,

$$\bar{y}_{ii}(k)=\frac{\bar{S}_i^*(k)-\sum_{j=1\sim N,\,j\neq i}\left[V_i^2(k)-\bar{V}_i^*(k)\bar{V}_j(k)\right]\bar{y}_{ij}}{V_i^2(k)} \tag{4}$$

A window of *K* data points has *NK* values of $\bar{y}_{ii}$ and *N*(*N*-1)/2 values of $\bar{y}_{ij}$ to be estimated. Thus, there are totally $N^2-N+2NK$ real parameters to estimate. *K* data points can provide 2*NK* nodal power injection equations in real realm. Since $N^2-N+2NK>2NK$, there are insufficient equations to solve all parameters. In each window, if we may assume a constant power factor for each $\bar{y}_{ii}$, its conductance g_{ii} and susceptance b_{ii} of $\bar{y}_{ii}$ at two adjacent time points will satisfy

$$\frac{g_{ii}(k-1)}{b_{ii}(k-1)}=\frac{g_{ii}(k)}{b_{ii}(k)} \qquad (k=2\sim K) \tag{5}$$

Thus, *K*-1 more equations are added to each bus and the entire load area needs to solve 3*NK*-*N* equations. From equality (6), there is *K*=*N*.

$$N^2-N+2NK=3NK-N \tag{6}$$

It means that each time window needs to have at least *N* data points to be able to solve all parameters of the load area. For instance, for load areas with *N*=2, 3 and 4 boundary buses, we need at least the same numbers of data points to solve 10, 24 and 44 unknowns, respectively.

From (4), g_{ii} and b_{ii} are both functions of $\bar{y}_{ij}$'s ($i\neq j$). An error index on (5) is defined as

$$e_i^{in}(k)=g_{ii}(k-1)b_{ii}(k)-g_{ii}(k)b_{ii}(k-1) \tag{7}$$

The second optimization problem is formulated as (8) for estimating load area parameters by minimizing three weighted summation terms. g_{ij} and b_{ij} are estimated conductance and susceptance of $\bar{y}_{ij}$; the 2nd and 3rd terms respectively summate their normalized differences from the previous time window; ω_{pf} and ω_y are the weighting factors respectively for variances of the power factor and $\bar{y}_{ij}$ over the time window.

$$\min J^{in}=\sum_{k=2}^{K}\sum_{i=1}^{N}\frac{\omega_{pf}}{N}\left[e_i^{in}(k)\right]^2+\sum_{\substack{i,j=1\\ i\neq j}}^{N}\omega_y\left(\frac{g_{ij}}{g_{ijp}}-1\right)^2+\sum_{\substack{i,j=1\\ i\neq j}}^{N}\omega_y\left(\frac{b_{ij}}{b_{ijp}}-1\right)^2$$

$$s.t. \quad g_{ij}>0 \tag{8}$$

The SQP method is also used to solve all $\bar{y}_{ij}$'s for each time window. Then, calculate load admittance $\bar{y}_{ii}$ directly by (4).

For this second optimization on estimation of load area parameters, initial values of g_{ij} and b_{ij} are also required, which can be obtained directly from the reduced bus admittance matrix about the load area by eliminating all buses except boundary buses.

C. Solving the Power Transfer Limit of each Tie Line

From real-time estimates of equivalent parameters, the active power transfer limit of each tie line can be solved analytically as a function of equivalent parameters.

The admittance matrix of the load area of the equivalent system is given in (9), where $\bar{Y}_{ij}=\bar{Y}_{ji}=-\bar{y}_{ij}$ and $\bar{Y}_{ii}=\sum_{j=1}^{N}\bar{y}_{ij}$.

$$\mathbf{Y}=\begin{bmatrix}\bar{Y}_{11} & \cdots & \bar{Y}_{1i} & \cdots & \bar{Y}_{1N}\\ \vdots & \ddots & & & \vdots\\ \bar{Y}_{i1} & & \bar{Y}_{ii} & & \bar{Y}_{iN}\\ \vdots & & & \ddots & \vdots\\ \bar{Y}_{N1} & \cdots & \bar{Y}_{Ni} & \cdots & \bar{Y}_{NN}\end{bmatrix} \tag{9}$$

Let $\mathbf{Y_E}$ be a column vector about all admittances $\bar{y}_{Ei}=1/\bar{z}_{Ei}$ (*i*=1~*N*) and $\mathbf{Y_E^D}$ be a diagonal matrix created from $\mathbf{Y_E}$, i.e.

$$\mathbf{Y_E}=[\bar{y}_{E1}\quad \bar{y}_{E2}\quad \cdots\quad \bar{y}_{EN}]^T \tag{10}$$

$$\mathbf{Y_E^D}=diag(\mathbf{Y_E})=\begin{bmatrix}\bar{y}_{E1} & & 0\\ & \ddots & \\ 0 & & \bar{y}_{EN}\end{bmatrix} \tag{11}$$

A vector about the injected currents satisfies

$$\mathbf{I}=\bar{E}\mathbf{Y_E}-\mathbf{Y_E^D}\mathbf{V} \tag{12}$$

where $\mathbf{V}=[\bar{V}_1\quad \bar{V}_2\quad \cdots\quad \bar{V}_N]^T$. Then, there is

$$\mathbf{V}=\bar{E}(\mathbf{Y}+\mathbf{Y_E^D})^{-1}\mathbf{Y_E}=\bar{E}\frac{\mathrm{adj}(\mathbf{Y}+\mathbf{Y_E^D})}{\det(\mathbf{Y}+\mathbf{Y_E^D})}\mathbf{Y_E} \tag{13}$$

For simplicity, let α_i denote the *i*-th element of $\mathrm{adj}(\mathbf{Y}+\mathbf{Y_E^D})\mathbf{Y_E}$ and let $\gamma=\det(\mathbf{Y}+\mathbf{Y_E^D})$. There is

$$\bar{V}_i=\bar{E}\alpha_i/\gamma \tag{14}$$

The complex power transferred on each tie line is a function of elements of $\mathbf{Y}$, $\bar{E}$ and $\mathbf{Y_E}$.

$$\mathbf{S}=[\bar{S}_1\quad \bar{S}_2\quad \cdots\quad \bar{S}_N]^T=(\bar{E}\mathbf{Y_E^D}-\mathbf{V^D}\mathbf{Y_E^D})^*\mathbf{V} \tag{15}$$

where $\mathbf{V^D} = diag(\mathbf{V})$. If changes on the external system are ignored, each complex power is a function of load admittances, i.e.

$$\bar{S}_i(\bar{y}_{11},\cdots,\bar{y}_{NN}) = (\bar{E}^*\bar{y}_{Ei}^* - \bar{y}_{Ei}^*\bar{V}_i^*)\bar{V}_i = \left|\bar{E}\right|^2 (\bar{y}_{Ei}^* - \bar{y}_{Ei}^*\frac{\alpha_i^*}{\gamma^*})\frac{\alpha_i}{\gamma} \quad (16)$$

$$P_i(\bar{y}_{11},\cdots,\bar{y}_{NN}) = \left|\bar{E}\right|^2 \mathrm{Re}\left[(\bar{y}_{Ei}^* - \bar{y}_{Ei}^*\frac{\alpha_i^*}{\gamma^*})\frac{\alpha_i}{\gamma}\right] \quad (17)$$

Based on the aforementioned constant power factor assumption over a time window for each load, P_i is a function of all load admittance magnitudes, i.e. y_{jj} (j=1~N). Its maximum $P_{i,j}^{\mathrm{Max}}$ with respect to the change of y_{jj} at bus j is reached when

$$\frac{\partial P_i(y_{11},\cdots,y_{NN})}{\partial y_{jj}} = 0 \qquad i, j=1\sim N \quad (18)$$

If an analytical solution of y_{jj} is obtained from (18) as a function of equivalent parameters, an analytical expression of $P_{i,j}^{\mathrm{Max}}$ can be derived by plugging the solution of y_{jj} into (17). $P_{i,i}^{\mathrm{Max}}$ with i=j represents the maximum active power transfer to bus i with only the local load at bus i varying; $P_{i,j}^{\mathrm{Max}}$ with $j\neq i$ represents the maximum active power transfer to bus i with only the load at another bus j varying.

For a general N+1 buses equivalent, the analytical solution of $P_{i,j}^{\mathrm{Max}}$ can be obtained by solving a quadratic equation. The proof based on (18) is given in the Appendix.

This paper assumes that each y_{jj} may change individually, so there are N such transfer limits $P_{i,1}^{\mathrm{Max}} \sim P_{i,N}^{\mathrm{Max}}$ for each tie line. By estimating the real-time pattern of load changes, the limit matching best that pattern will be more accurate and selected. Voltage stability margin on a tie line is defined as the difference between the limit and the real-time power transfer.

III. Online Scheme for Implementation

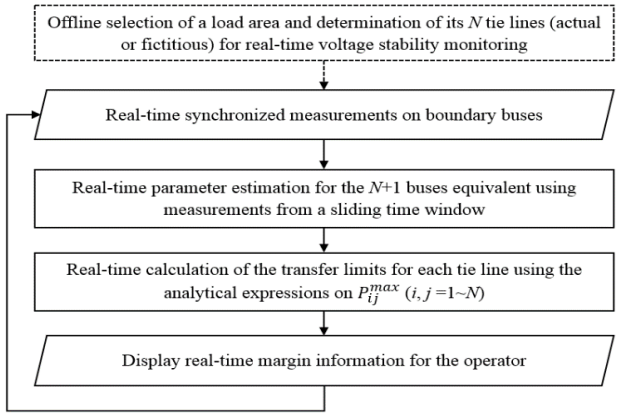

Fig. 2. Flowchart of the new method.

Compared with the traditional TE-based approach, this new measurement-based method uses a more complex N+1 buses equivalent to model more details about the boundary of a load area. Synchronized measurements on all boundary buses are needed from either state estimation results if only steady-state voltage instability is concerned or PMUs for real-time detection of voltage instability. The parameters of the equivalent are identified using real-time measurements over a recent time window for several seconds. In a later case study on the NPCC system, results from 5s and 10s time windows will be compared. If the scheme uses PMUs, in order to speed up online parameter identification and filter out noise or dynamics irrelevant to voltage stability, the original high-resolution measurements (e.g. at 30Hz) may be downgraded to a low-sampling rate f_s (e.g. 2Hz) by averaging the raw data over a time internal of $1/f_s$ (i.e. 0.5s for 2Hz).

As shown by the flowchart in Fig. 2, the new method first identifies all branches connecting the load area with the rest of the system, which comprise a cut set partitioning the load area. Those branches are assumed coming from the same voltage source $\bar{E}$. Then, any branches coming to the same boundary buses are merged. Assume that M branches are yielded. The proposed method is able to calculate the transfer limit for each branch using an M+1 buses equivalent. However, if M is large, it will result in huge computational burdens in estimating $M(M\text{-}1)/2+2M+1$ parameters and consequently calculating M limits. Different from the TE that merging all M branches to one fictitious tie line, this new approach may group some branches across the boundary and only merge each group to one fictitious tie line. The criteria of grouping are such as: the boundary buses in one group are tightly interconnected; the branches in one group reach limits almost at the same time; it is not required to monitor the branches within a group individually. For the fictitious tie line representing a group of branches, only its total limit is calculated. Thus, after merging some groups of branches to fictitious tie lines, the final number of tie lines becomes N<M. A simpler N+1 buses equivalent is used, which still keeps characteristics of the load area regarding voltage stability. The TE-based approach is a special case of this new method with N=1.

The next two sections will test the new method on a 4-bus power system and the NPCC 140-bus system using data generated from simulation. All computations involved in the algorithms of the new method are performed in MATLAB on an Intel Core i7 CPU desktop computer.

IV. Demonstration on a 4-bus Power System

This section demonstrates the new method on a 4-bus power system with one constant voltage source supporting three interconnected load buses representing a load area. The system is simulated in MATLAB with gradual load increases at three load buses. The simulation results on three load buses are treated as PMU data and fed to the new method. The system represents a special case of the system in Fig. 1 with N=3. Let $\bar{E} = 1.0\angle 5^\circ$ pu and three tie lines have the same impedance $\bar{z}_{E1} = \bar{z}_{E2} = \bar{z}_{E3} = 0.01 + j0.1$ pu. At the beginning, three load impedances $\bar{z}_{11} = \bar{z}_{22} = \bar{z}_{33} = 1+j1$ pu. Consider two groups of transfer impedances in Table I respectively for weak and tight connections between three boundary buses.

TABLE I Values of Transfer Impedances

Group	$\bar{z}_{12}$ (pu)	$\bar{z}_{13}$ (pu)	$\bar{z}_{23}$ (pu)
A	0.01+j0.1	0.015+j0.15	0.005+j0.05
B	0.0005+j0.005	0.0008+j0.0075	0.0003+j0.0025

Keep the impedance angle of $\bar{z}_{33}$ unchanged but gradually

reduce its modulus by 1% every 2s until active powers on all tie lines meet limits. As shown in Fig 3, three PV curves (P_i vs. V_i) are drawn for two groups of transfer impedances. For Group A, the transfer impedances between boundary buses are not ignorable compared with the tie-line and load impedances, so three PV curves are distinct. However, when those impedances decrease to the values in Group B, three PV curves basically coincide, which is the case a TE can be applied to.

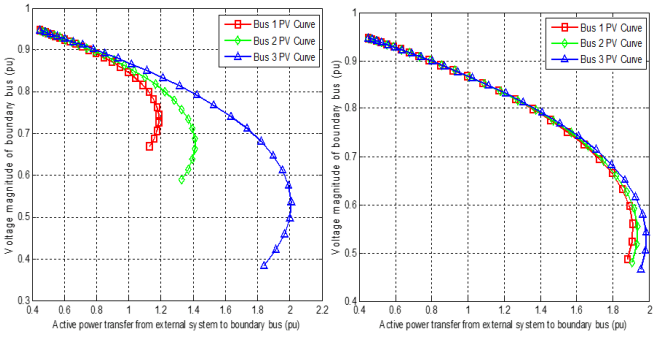

(a) Group A (weak). (b) Group B (tight).

Fig. 3. PV curves for weak and tight connections between boundary buses.

Simulation results are recorded at 1Hz sampling rate. The new method is performed every 1s using the data of the latest 10s time window. All computation of the new method on each time window is finished within 0.05s in MATLAB. The new method gives each tie line three limits for three extreme load increase assumptions. For two groups, Fig. 4 and Fig. 5 show P_1~P_3, the total tie-line flow $P_\Sigma=P_1+P_2+P_3$, and their limits calculated by the new method. The limits from solutions of $\partial P_1/\partial y_{33}$ ~$\partial P_3/\partial y_{33}$ match the actual load increase, so their sum is defined as the total tie-line flow limit $P_\Sigma^{\text{Max(New)}}$. For comparison, the TE-based method in [20] and [21] is also performed to give the total tie-line flow limit as $P_\Sigma^{\text{Max(TE)}}$ in Fig. 4.

Tests on those two groups of data show that when a TE-based method is applied to a load area, voltage instability is detected only when the total tie-line flow meets its limit. However, due to the uneven increase of load, one tie line may be stressed more to reach its limit earlier than the others, which can successfully be detected by the new method. Another observation on Fig. 4 and Fig. 5 is that the curve of $P_\Sigma^{\text{Max(New)}}$ is flatter than that of $P_\Sigma^{\text{Max(TE)}}$, and $P_\Sigma^{\text{Max(TE)}}$ is more optimistic and less accurate than $P_\Sigma^{\text{Max(New)}}$ when the system has a distance to voltage instability.

For Group A with weak interconnection between boundary buses, Fig. 4 shows that three individual tie-line flows P_1, P_2 and P_3 meet their limits at t=680s, 676s and 666s respectively. The total tie-line flow P_Σ meets $P_\Sigma^{\text{Max(New)}}$ at t=680s. $P_\Sigma^{\text{Max(TE)}}$ from the TE-based method is not as flat as $P_\Sigma^{\text{Max(New)}}$, and it is met by P_Σ after t=700s. Fig. 6-Fig. 8 give details of Fig. 4 on each tie-line flow and its three limits calculated according to (18) for three load increase assumptions. The limit from solution of $\partial P_i/\partial y_{33}$ matches the actual load increase, and its curve is flat and met by P_i earlier than the other two. By using the new method, zero margin is first detected at t=666s on the 3rd tie line and then on the other two tie lines as well as the total tie-line flow. However, the TE-based method detects zero margin much later since, first, it only monitors the total tie-line flow limit and second, the limit curve is not as flat as that given by the new method.

For Group B with tight connection between boundary buses, Fig. 5 shows that all tie-line flows reach their limits at t=732s. Also, P_Σ meets both $P_\Sigma^{\text{Max(New)}}$ and $P_\Sigma^{\text{Max(TE)}}$ at that same time.

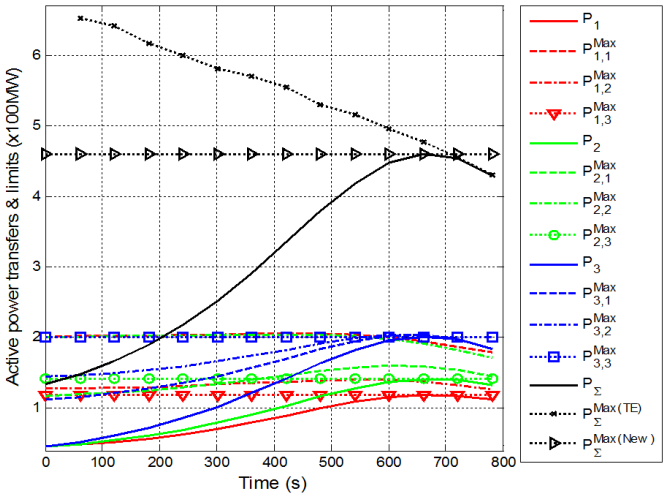

Fig.4. Tie-line flows and limits for Group A (weak connection).

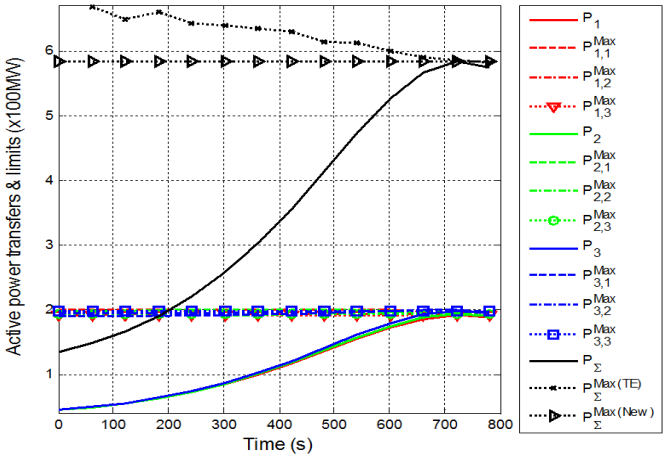

Fig. 5. Tie-line flows and limits for Group B (tight connection).

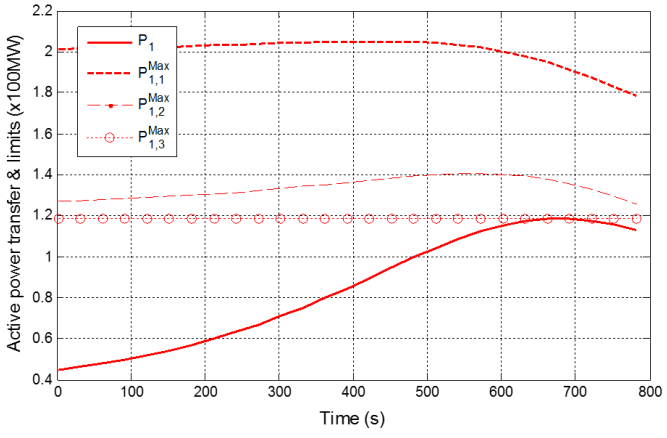

Fig. 6. P_1 and limits for Group A.

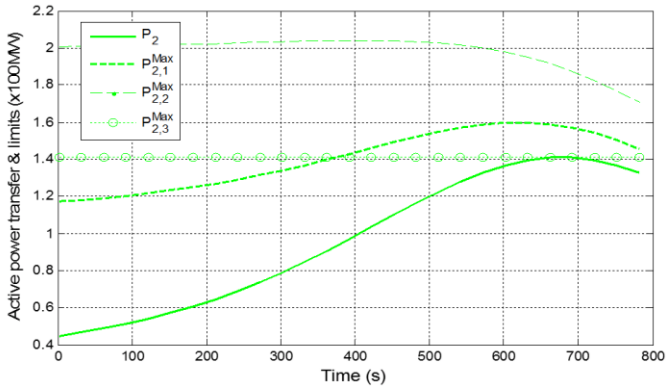

Fig. 7. P_2 and limits for Group A.

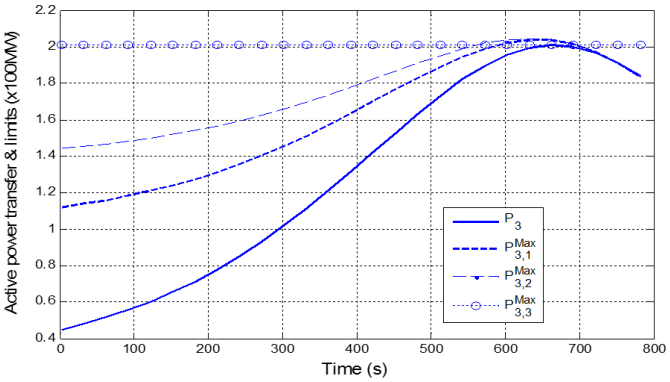

Fig. 8. P_3 and limits for Group A.

V. Case Studies on the NPCC Test System

The proposed new method is tested on a Northeast Power Coordinating Council (NPCC) 48-machine, 140-bus system model [27]. As highlighted in Fig. 9, the system has a Connecticut Load Center (CLC) area supported by power from three tie lines, i.e. 73-35, 30-31 and 6-5. Line 73-35 is from the NYISO region and the other two are from the north of the ISO-NE region. Powertech's TSAT is used to simulate four voltage instability scenarios about the CLC area:

A. Generator trip followed by load increase leading to voltage instability;
B. Generator trip followed by a tie-line tip causing voltage instability;
C. Two successive tie-line trips causing voltage instability;
D. Shunt switching to postpone voltage instability.

The load model at each load bus adopts the default load model setting in TSAT, i.e. 100% constant current for real power load and 100% constant impedance for reactive power load. Simulation results on the voltages at boundary buses 35, 31 and 5 and the complex powers of the three tie lines are recorded at 30Hz, i.e. the typical PMU sampling rate. The raw data are preprocessed by an averaging filter over 15 samples to be downgraded to 2Hz. The processed data are then fed to the new method for estimating the external and load area parameters and calculating transfer limits. That data preprocessing improves the efficiency of two optimizations for parameter estimation while keeping necessary dynamics on voltage stability in data. The new method is performed every 0.5s on data of the latest 5s time window.

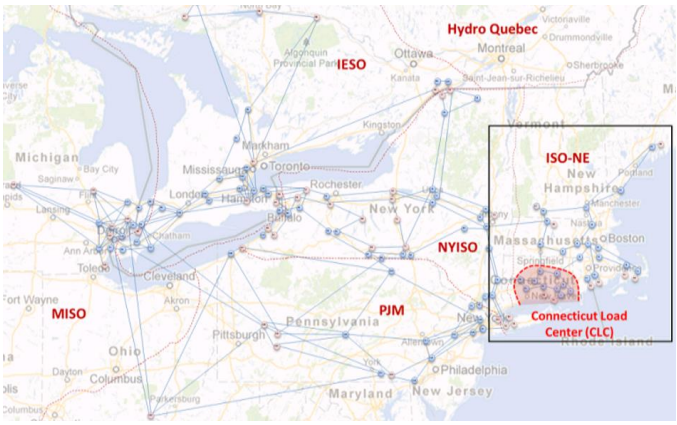

(a) System topology.

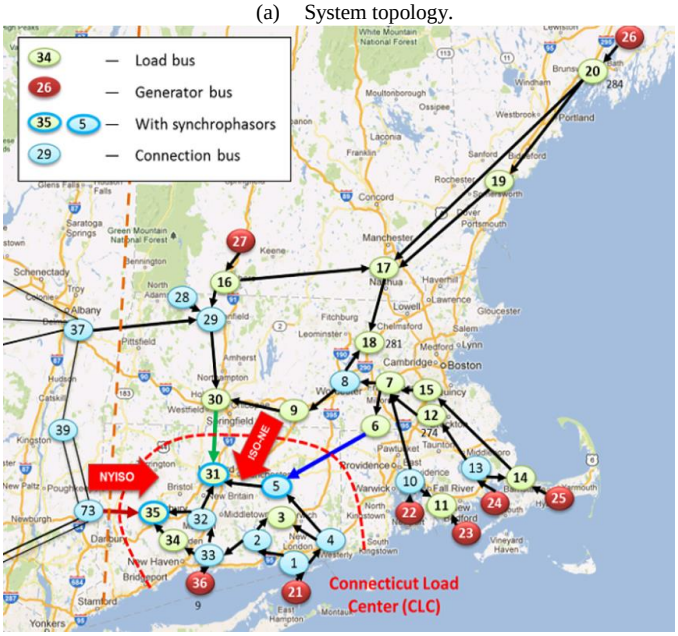

(b) CLC area.

Fig. 9. Map of NPCC system and CLC area.

A. Generator Trip Followed by Load Increase Leading to Voltage Instability

To create voltage collapse in the CLC area, all its loads are uniformly increased by a total of 0.42 MW per second from its original load of 1906.5 MW with constant load power factors. At t=360s, the generator on bus 21 is tripped, which pushes the system to be close to the voltage stability limit. Shortly after slight load increase, voltage collapse happens around t=530s as shown in Fig. 10 on three boundary bus voltages. Fig. 11 indicates the PV curves monitored at three boundary buses. To better illustrate the PV curves, the figure is drawn using the data sampled at 25s intervals until t=500s to filter out transient dyanmics on the curves right after the generator trip and the voltage collapse at the end. Note that the generator trip causes a transition from the pre-contingency PV curves to the post-contingency PV curves with a more critical condition of voltage stability. Bus 35 is the most critical bus since the "nose point" of its post-contigency PV curve is passed.

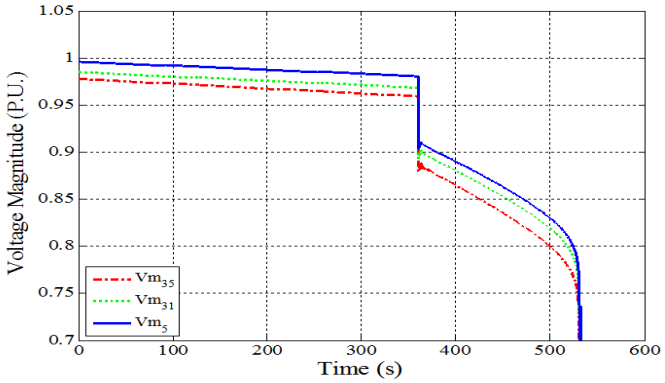

Fig. 10. Voltage magnitudes at CLC boundary buses.

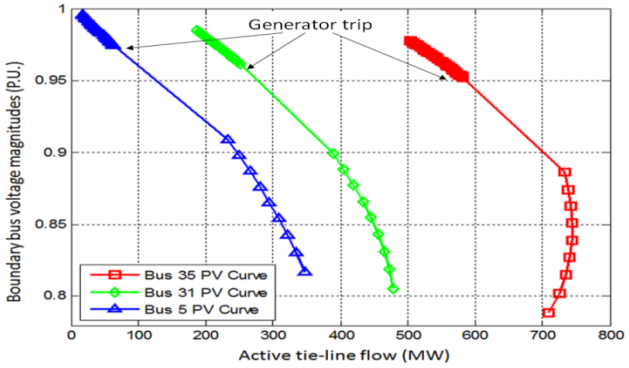

Fig. 11. PV curves monitored at the CLC boundary buses.

When the external system has strong coherency, the proposed new method can be applied to reduce it to one voltage phasor $\bar{E}$ connected with boundary buses of the load area by N branches, respectively. Fig. 12 and Fig. 13 show the voltage magnitudes and angles of all buses in Fig. 9(b) that are outside the CLC load center, indicating a strong coherency of the external system. Therefore, the proposed method is valid and may adopt a 3+1 buses equivalent to calculate the power transfer limits separately for three tie lines.

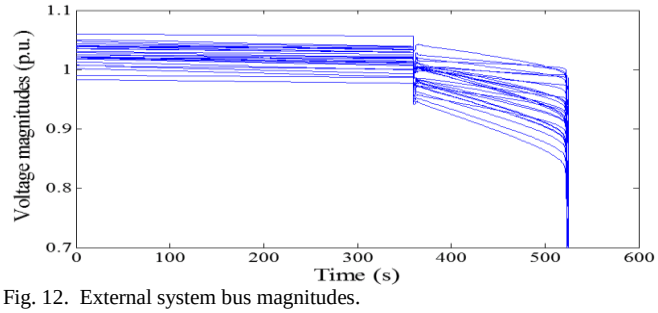

Fig. 12. External system bus magnitudes.

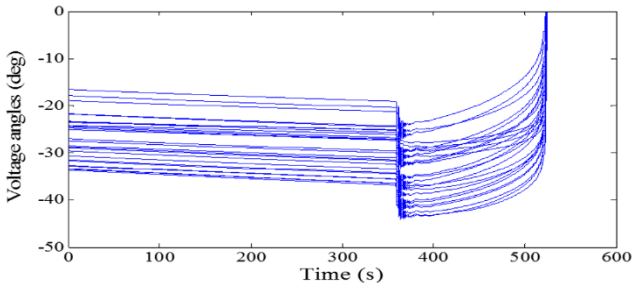

Fig. 13. External system bus angles.

Fig. 14 gives estimates of three load impedance magnitudes seen at the boundary buses. The figure shows that the load seen from bus 5 changes more siginificantly than the others. Hence, $P_{35,5}^{\mathrm{Max}}$, $P_{31,5}^{\mathrm{Max}}$ and $P_{5,5}^{\mathrm{Max}}$ calculated from $\partial P_i/\partial y_5=0$ are more accurate and used to calculate stability margin.

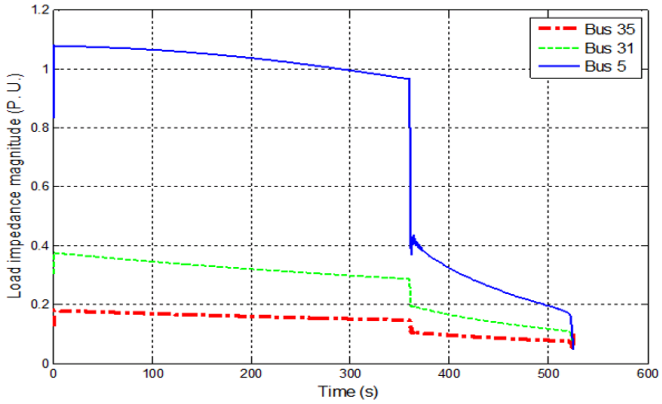

Fig. 14. Real-time estimation of load impedance magnitudes.

To compare with the new method, Fig. 15 gives the total transfer limit estimated using a TE-based method. The margin stays positive until the final collapse of the entire system.

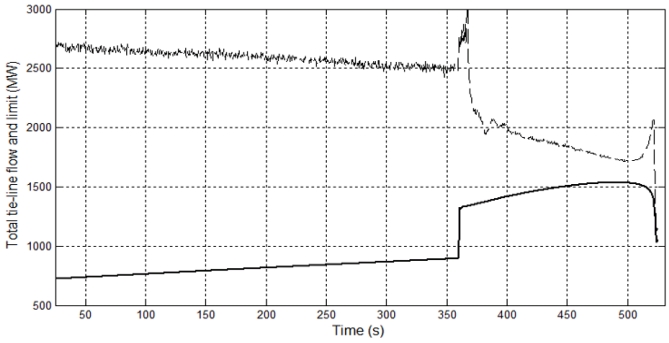

Fig. 15. Result from a TE-based method.

Fig. 16 gives the results from the new method and each tie line has three transfer limits. Before the generator trip, all lines have sufficient margins to their limits. After the trip, more power is needed from the external system, so the active powers of the three tie lines all increase significantly to approach to their limits. In Fig. 16(a), P_{35} of 73-35 reaches the limit $P_{35,5}^{\mathrm{Max}}$ at t=473.5s. From Fig. 16 (b) and (c), the other two lines keep positive margins until the final voltage collapse. It confirms the observation from Fig. 11 that voltage collapse will initiate from bus 35. If the limit and margin information on individual tie line is displayed for operators in real time, an early remedial action may be taken before voltage collapse. However, such information is not available from a TE-based method.

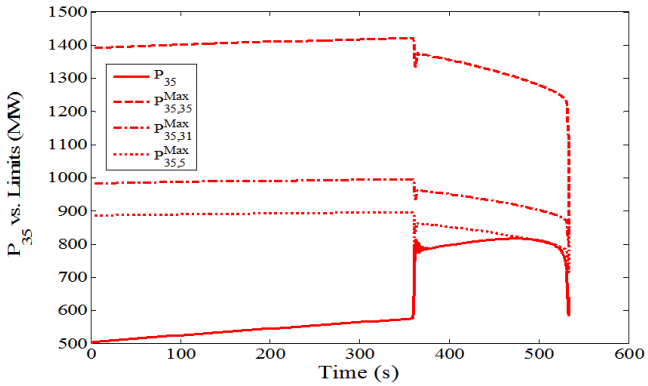

(a) P_{35} vs. its limits.

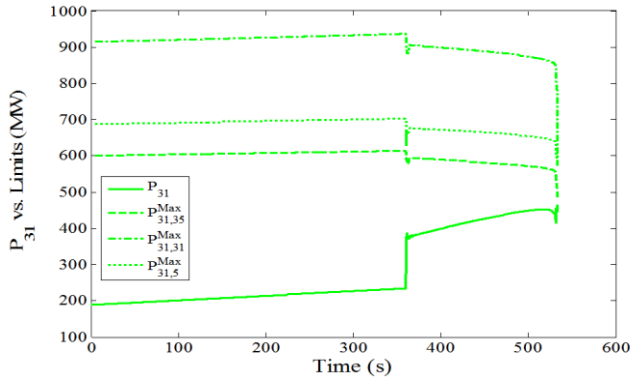

(b) P_{31} vs. its limits.

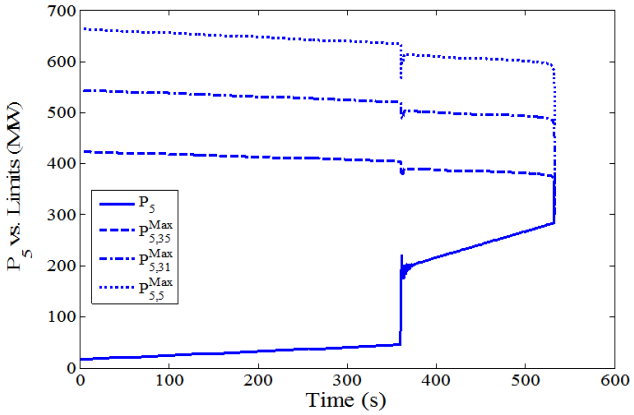

(c) P_5 vs. its limits.

Fig. 16. Transfer limits of each tie line calculated by the new approach.

Once parameters of the N+1 buses equivalent are estimated, transfer limits are directly calculated by their analytical expressions. The major time cost of the new method is with online parameter estimation. Fig. 17 gives the probability density about the times spent respectively on estimating the external system and the load area over one time window. According to the figure, parameter estimation over one time window can be accomplished within 0.02s to 0.1s. The average total time cost for each cycle of the new method's online procedure (i.e. steps 2-5 in Fig. 2) is 0.0614s, which includes 0.0221s for external parameter estimation, 0.0271s for load area parameter estimation, and 0.0122s for transfer limits calculation. The times on measurements input and margin display are ignorable. The test results indicate that the new method can be applied in an online environment.

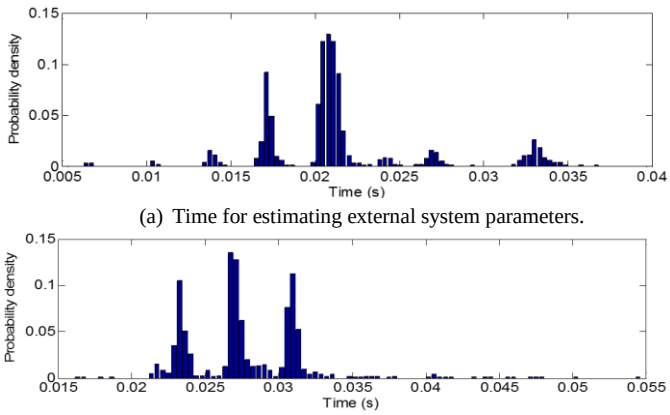

(a) Time for estimating external system parameters.

(b) Time for estimating load area parameters.

Fig. 17. Time performances on online parameter estimation.

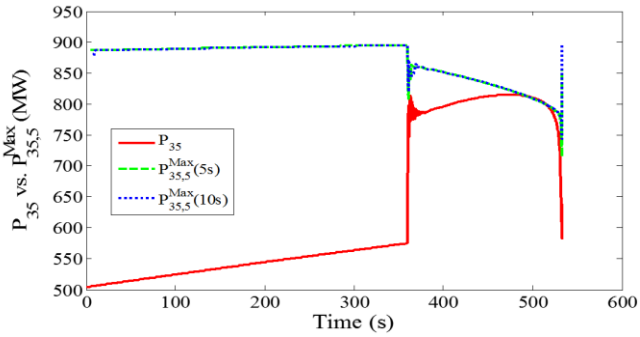

Fig. 18. Comparison of different optimization time windows.

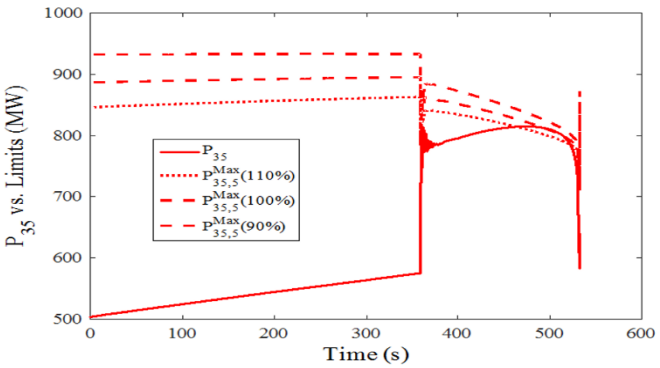

Fig. 19. Comparison of initial values with errors.

Fig. 18 compares the estimated $P_{35,5}^{\mathrm{Max}}$ using a 5s sliding time window with that using a 10s sliding window. Two results match very well, which indicates that the new method is not very sensitive to the length of the sliding time window.

To test the results of the new method using inaccurate initial values in the external system parameter estimation, Fig. 19 compares the tie-line power limits for 73-35 with three different sets of initial values: 110%, 100% and 90% of the estimates from a Least Square method on the first time window at the beginning. From the figure, a 10% error will cause less than 5% error in the transfer limit estimation before the generator trip and about 2% error in the limit after the generator trip. If the Least Square method is used to re-estimate the initial values when the generator trip is detected, that 2% error can be eliminated and these three limits will merge to one limit associated with accurate initial values. Considering in the

real world, small errors in the initial values cannot be avoided completely, a small positive threshold rather than zero may be defined for the transfer margin as an alarm of voltage instability.

B. Generator Trip Followed by a Tie-Line Tip Causing Voltage Instability

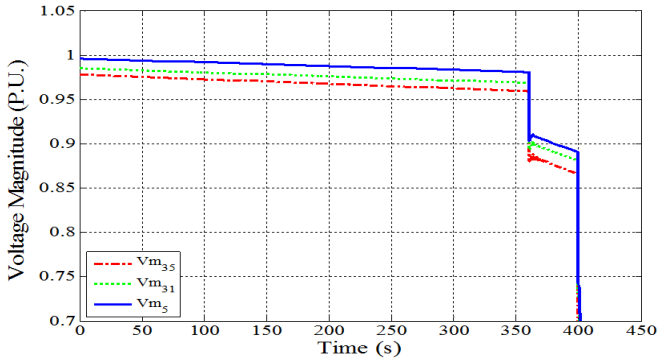

Fig. 20. Voltage magnitudes at CLC boundary buses.

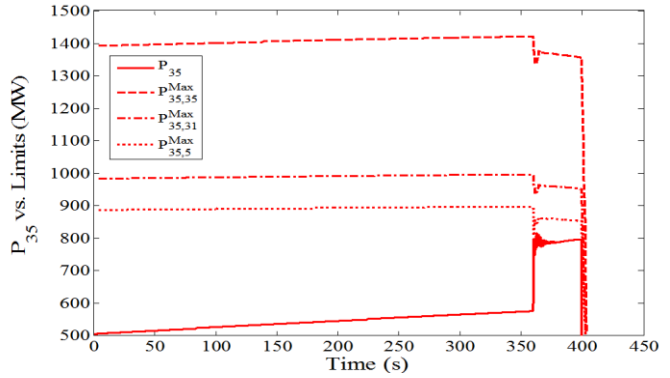

(a) P_{35} vs. its limits.

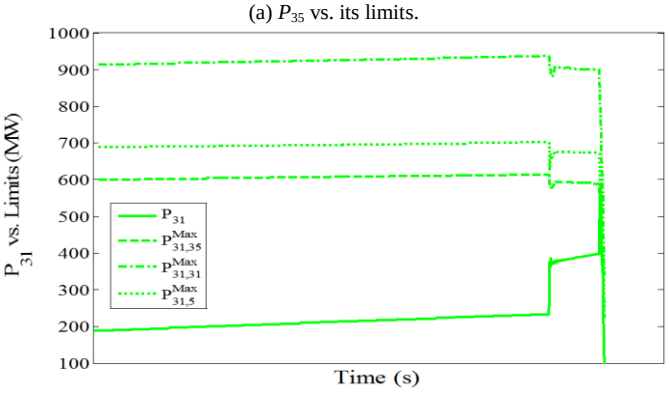

(b) P_{31} vs. its limits.

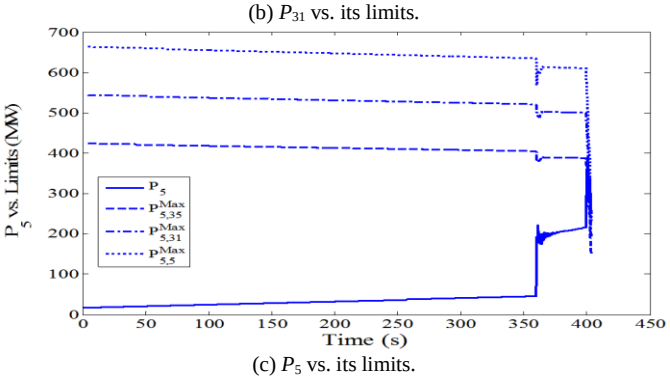

(c) P_5 vs. its limits.

Fig. 21. Transfer limits of each tie line calculated by the new approach.

Before t=400s, this scenario is the same as Scenario B. At t=400s, tie-line 73-35 is tripped to cause voltage collapse immediately. The voltage magnitudes of three boundary buses are shown in Fig. 20.

Fig. 21 shows the tie-line power flows and their limits for this scenario. After the generator trip, all tie-line flows become closer to their limits, and tie-line 73-35 carries 795 MW, which is higher than the total margin of 667MW on tie-lines 31-30 and 6-5. When tie-line 73-35 is tripped at t=400s, its flow is transferred to the other two tie lines to cause them to meet limits. That explains why voltage collapse happens following that tie-line trip. If the above tie-line margin information is presented to the system operator before t=400s, the operator will be aware of that the system following the generator trip cannot endure such a single tie-line trip contingency and may take a control action.

C. Two Successive Tie-line Trips Causing Voltage Instability

In this scenario, two successive tie-line trips on 31-30 and 6-5 are simulated to test the adaptability of the new method to "N-1" and "N-2" conditions. During t=0-100s, all loads in CLC area are uniformly increased by 0.43MW/s from its original load of 1906.5 MW with constant power factors unchanged. At t=100s, the tie-line 31-30 is tripped, and thus the voltages of three boundary buses drop significantly. During t=100-200s, loads keep increasing at a lower speed equal to 0.37MW/s. At t=200s, the tie-line 6-5 is tripped, causing voltage collapse as shown in Fig. 22.

Fig. 23 gives the results on each tie line and the transfer limits. Before tie-line 31-30 is tripped at t=100s, all tie lines have sufficient transfer margin. After that trip, P_{31}=0 is captured from measurements and the new method sets the corresponding y_{E31}=0 to adapt to the new "N-1" condition. Then, the transfer limit on tie-line 73-35 drops to 677 MW. Before the next tie-line 6-5 is tripped at t=200s, tie-lines 73-35 and 6-5 totally transfer 733MW to the CLC area, which is higher than the limit 677 MW of tie-line 73-35. Therefore, the second tie-line trip causes zero margin on tie-line 73-35, followed by a voltage collapse.

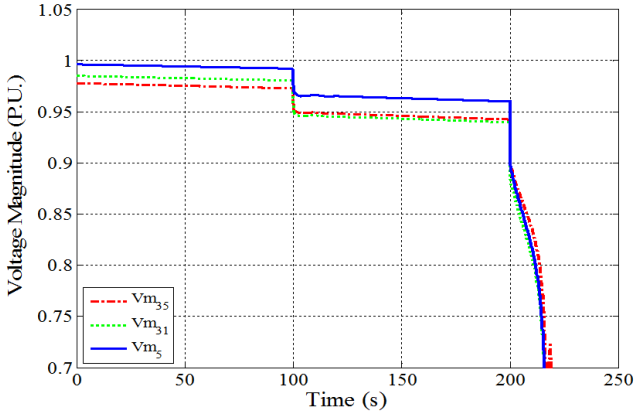

Fig. 22. Voltage magnitudes at CLC boundary buses.

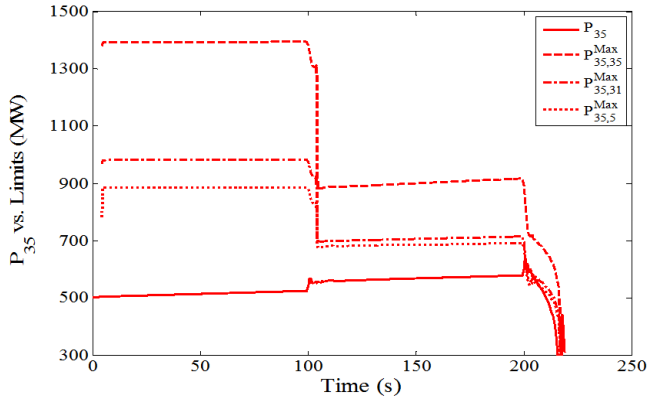

(a) P_{35} vs. its limits.

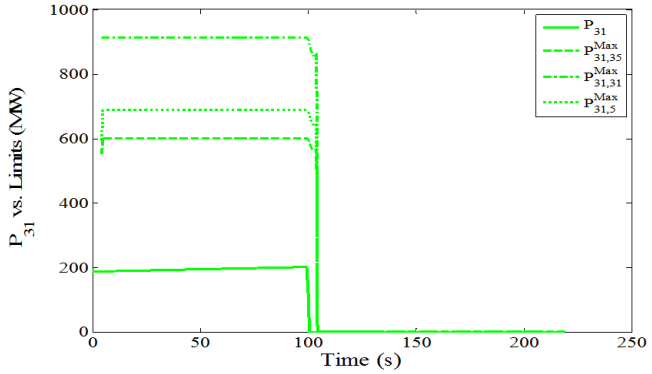

(b) P_{31} vs. its limits.

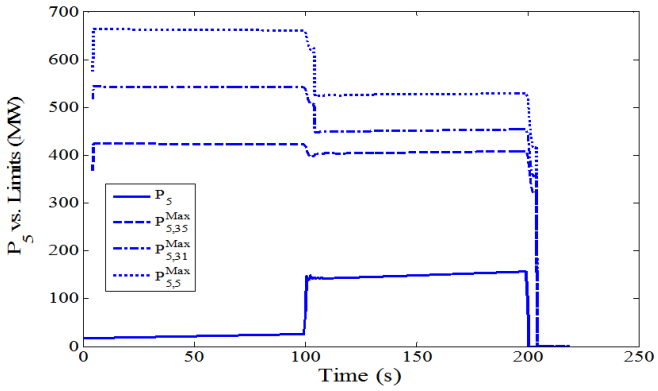

(c) P_5 vs. its limits.

Fig. 23. Transfer limits of each tie line calculated by the new approach.

D. Shunt Switching to Postpone Voltage Instability

This scenario considers switching in a capacitor bank located in the CLC area to postpone voltage collapse. Everything of this scenario during t=0-440s is the same as Scenario A. At t=440s when the transfer margin on the most critical tie-line 73-35 drops to 3%, a 50MVAR capacitor bank at bus 33 is switched in. Due to its additional VAR support, the voltage of the CLC area increases as shown in Fig. 24 about voltage magnitudes of three boundary buses. Fig. 25 shows the transfer limits on tie-line 73-35 for this scenario. Both the tie-line flow and limits increase after that switch. The slight tie-line flow increase is caused by voltage-sensitive loads in the load area, which is smaller than the increase of the limit. Therefore, zero margin happens at t=496.5s, i.e. 23s later than the 473.5s of Scenario A. This scenario demonstrates that adding VAR support in the load area will increase voltage stability margin, which is correctly captured by the new method.

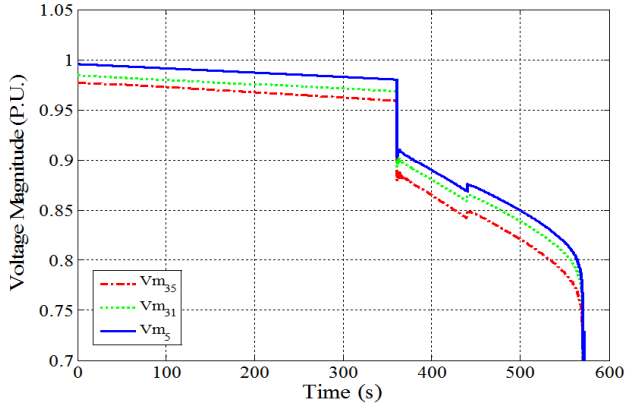

Fig. 24. Voltage magnitudes at CLC boundary buses.

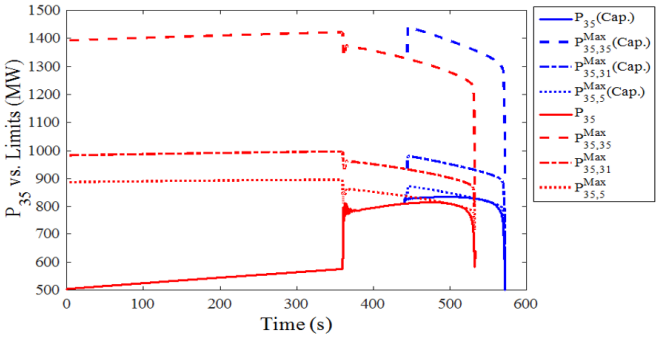

Fig. 25. P_{35} vs. its limits.

VI. Discussion and Conclusions

This paper has proposed a new measurement-based method for real-time voltage stability monitoring of a load area fed by multiple tie lines. The new method is based on an N+1 buses equivalent system, whose parameters are estimated directly from synchronized measurements obtained at the boundary buses of the load area. For each tie line, the method calculates the transfer limit and margin against voltage instability analytically from that estimated equivalent system. The new method has been demonstrated in detail on a 4-bus system and then tested by case studies on a 140-bus NPCC system model.

Compared to a traditional TE-based method for measurement-based voltage stability monitoring, the new method has two apparent advantages. First, the new method offers detailed limit and margin information on individual tie lines so as to identify the tie line and boundary bus with the smallest margin as the location where voltage instability more likely initiates. Second, as demonstrated on the 4-bus system, before the voltage collapse point, the total tie-line flow limit from the new method is more accurate than the limit from the TE-based method. The latter fluctuates more and is not as flat as the former because the TE-based method does not model the weak or strong connection between boundary buses. The above second advantage makes the new method more suitable for online monitoring and early warning of voltage instability, and the first advantage can help the system operator to identify the location where voltage instability more likely initiates and accordingly choose more effective control resources, e.g., those having shorter electrical distances to the tie line with the

smallest margin. In our future work, voltage stability control based on the proposed new method will be studied.

VII. Appendix

Theorem: an analytical solution of $P_{i,j}^{\text{Max}}$ can be obtained by solving a quadratic equation.

Proof: As defined above, α_i represents the *i*-th element of $\text{adj}(\mathbf{Y}+\mathbf{Y_E^D})\mathbf{Y_E}$ and $\gamma=\det(\mathbf{Y}+\mathbf{Y_E^D})$. It is easy to know that they are both linear complex functions of the load admittance $\bar{y}_{jj}=y_{jj}e^{j\phi}$, where y_{jj} and ϕ are the magnitude and angle of $\bar{y}_{jj}$. So they can be represented as $\gamma=d_{j1}y_{jj}e^{j\phi}+d_{j2}$ and $\alpha_i=d_{j3}y_{jj}e^{j\phi}+d_{j4}$, where d_{j1}~d_{j4} are constant complex numbers (note that if $j=i$, y_{jj} does not appear in α_i, so $d_{j3}=0$).

Equation (18) becomes

$$\frac{\partial P_i(y_{jj})}{\partial y_{jj}}=\frac{E^2}{|\gamma|^4}\text{Re}\{\bar{y}_{Ei}^*[d_{j3}\gamma(\gamma^*)^2-d_{j3}\alpha_i^*\gamma\gamma^*-d_{j3}^*\alpha_i\gamma\gamma^* -d_{j1}\alpha_i(\gamma^*)^2+d_{j1}\alpha_i\alpha_i^*\gamma^*+d_{j1}^*\alpha_i\alpha_i^*\gamma]\}=0 \quad \text{(A1)}$$

where E^2 and $|\gamma|^4>0$. Then, an analytical solution of y_{ii} can be obtained by solving

$$\text{Re}\{\bar{y}_{Ei}^*[d_{j3}\gamma(\gamma^*)^2-d_{j3}\alpha_i^*\gamma\gamma^*-d_{j3}^*\alpha_i\gamma\gamma^* -d_{j1}\alpha_i(\gamma^*)^2+d_{j1}\alpha_i\alpha_i^*\gamma^*+d_{j1}^*\alpha_i\alpha_i^*\gamma]\}=0 \quad \text{(A2)}$$

It can be simplified into the form of a quadratic equation:

$$ay_{jj}^2+by_{jj}+c=0 \quad \text{(A3)}$$

where

$$a=\text{Re}\{y_{Ei}^*[(|d_{j1}|^2 d_{j3}d_{j4}^*-d_{j1}d_{j2}^*|d_{j3}|^2)e^{j\phi} +((d_{j1}^*)^2d_{j2}d_{j3}-d_{j1}(d_{j1}^*)^2d_{j4}-d_{j1}^*d_{j2}|d_{j3}|^2+|d_{j1}|^2 d_{j3}^*d_{j4})e^{-j\phi}]\}$$

$$b=\text{Re}\{2\bar{y}_{Ei}^*[|d_{j1}|^2|d_{j4}|^2-|d_{j2}|^2|d_{j3}|^2+d_{j1}^*|d_{j2}|^2 d_{j3}-|d_{j1}|^2 d_{j2}^*d_{j4}]\}$$

$$c=\text{Re}\{y_{Ei}^*[(d_{j2}(d_{j2}^*)^2d_{j3}-d_{j1}(d_{j2}^*)^2d_{j4}-|d_{j2}|^2 d_{j3}d_{j4}^*+d_{j1}d_{j2}^*|d_{j4}|^2)e^{j\phi} +(d_{j1}^*d_{j2}|d_{j4}|^2-|d_{j2}|^2 d_{j3}^*d_{j4})e^{-j\phi}]\}$$

The closed-form solution of (A3) can be derived and then plugged into (17) to obtain the analytical expression of $P_{i,j}^{\text{Max}}$. □

As an example, for N=3, to solve $P_{1,1}^{\text{Max}}$ and $P_{1,2}^{\text{Max}}$, define

$$\bar{y}_i \overset{\text{def}}{=} \bar{y}_{Ei}+\sum_{j=1\sim3}\bar{y}_{ij} \qquad i=1\sim3 \quad \text{(A4)}$$

All involved *d*-constants, d_{11}, d_{12}, d_{13}, d_{14}, d_{21}, d_{22}, d_{23} and d_{24} are

$$d_{11}=\bar{y}_2\bar{y}_3-\bar{y}_{23}^2 \quad \text{(A5)}$$

$$d_{12}=d_{11}(\bar{y}_{E1}+\bar{y}_{12}+\bar{y}_{13})-\bar{y}_{12}^2\bar{y}_3-\bar{y}_{13}^2\bar{y}_2-2\bar{y}_{12}\bar{y}_{13}\bar{y}_{23} \quad \text{(A6)}$$

$$d_{13}=0 \quad \text{(A7)}$$

$$d_{14}=d_{11}\bar{y}_{E1}+(\bar{y}_{12}\bar{y}_3+\bar{y}_{13}\bar{y}_{23})\bar{y}_{E2}+(\bar{y}_{12}\bar{y}_{23}+\bar{y}_{13}\bar{y}_2)\bar{y}_{E3} \quad \text{(A8)}$$

$$d_{21}=\bar{y}_1\bar{y}_3-\bar{y}_{13}^2 \quad \text{(A9)}$$

$$d_{22}=d_{21}(\bar{y}_{E2}+\bar{y}_{12}+\bar{y}_{23})-\bar{y}_{12}^2\bar{y}_3-\bar{y}_{23}^2\bar{y}_1-2\bar{y}_{12}\bar{y}_{13}\bar{y}_{23} \quad \text{(A10)}$$

$$d_{23}=\bar{y}_{E1}\bar{y}_3+\bar{y}_{E3}\bar{y}_{13} \quad \text{(A11)}$$

$$d_{24}=d_{23}(\bar{y}_{E2}+\bar{y}_{12}+\bar{y}_{23})-\bar{y}_{23}^2\bar{y}_{E1}+\bar{y}_{12}\bar{y}_{23}\bar{y}_{E3}+(\bar{y}_{12}\bar{y}_3+\bar{y}_{13}\bar{y}_{23})\bar{y}_{E2} \quad \text{(A12)}$$

Note that $\bar{y}_{11}$ does not appear in d_{11}~d_{14} and $\bar{y}_{22}$ does not appear in d_{21}~d_{24}.

VIII. References

[1] W. Taylor, Power System Voltage Stability: McGraw-Hill, 1994.

[2] T. Van Cutsem, L. Wehenkel, et al., "Decision tree approaches to voltage security assessment," *IEE Proceedings C Generation, Transmission and Distribution*, vol. 140, no. 3, pp. 189-198, 1993.

[3] R. Diao, K. Sun, V. Vittal et al., "Decision tree-based online voltage security assessment using PMU measurements," *IEEE Trans. Power Systems*, vol. 24, no. 2, pp. 832-839, 2009.

[4] K. Vu, M. M. Begovic, D. Novosel et al., "Use of local measurements to estimate voltage-stability margin," *IEEE Trans. Power Systems*, vol. 14, no. 3, pp. 1029-1035, 1999.

[5] I. Smon, G. Verbic, F. Gubina, "Local voltage-stability index using tellegen's Theorem," *IEEE Trans. Power Systems*, vol. 21, no. 3, pp. 1267-1275, 2006.

[6] B. Milosevic, M. Begovic, "Voltage-stability protection and control using a wide-area network of phasor measurements," *IEEE Trans. Power Systems*, vol. 18, no. 1, pp. 121-127, 2003.

[7] B. Leonardi, V. Ajjarapu, "Development of multilinear regression models for online voltage stability margin estimation," *IEEE Trans. Power Systems*, vol. 26, no. 1, pp. 374-383, 2011.

[8] M. Parniani, et al., "Voltage stability analysis of a multiple-infeed load center using phasor measurement data." *IEEE PES Power Systems Conference and Exposition*, Nov 2006.

[9] S. Corsi, and G. N. Taranto, "A real-time voltage instability identification algorithm based on local phasor measurements," *IEEE Trans. Power Systems*, vol. 23, no. 3, pp. 1271-1279, 2008.

[10] C. D. Vournas, and N. G. Sakellaridis, "Tracking maximum loadability conditions in power systems." *in Proc. 2007 Bulk Power System Dynamics and Control-VII*, Charleston, SC, Aug. 2007.

[11] M. Glavic, and T. Van Cutsem, "Wide-area detection of voltage instability from synchronized phasor measurements. Part I: Principle," *IEEE Trans. Power Systems*, vol. 24, no. 3, pp. 1408-1416, 2009.

[12] C. Vournas, C. Lambrou, M. Glavic et al., "An integrated autonomous protection system against voltage instability based on load tap changers." *2010 iREP Symposium*, Aug. 2010

[13] S. M. Abdelkader, D. J. Morrow, "Online Thévenin equivalent determination considering system side changes and measurement errors," *IEEE Trans. Power Systems*, vol. PP, no. 99, pp. 1-10, 2014.

[14] L. He, C.-C. Liu, "Parameter identification with PMUs for instability detection in power systems with HVDC integrated offshore wind energy," *IEEE Trans. Power Systems*, vol. 29, no. 2, pp. 775-784, 2014.

[15] W. Li, et al., "Investigation on the Thevenin equivalent parameters for online estimation of maximum power transfer limits," *IET Generation, Transmission & Distribution*, vol. 4, no. 10, pp. 1180-1187, 2010.

[16] Y. Wang, I.R. Pordanjani, et al, "Voltage stability monitoring based on the concept of coupled single-port circuit," *IEEE Trans. Power Systems*, vol. 26, no. 4, pp. 2154-2163, 2011.

[17] J.-H. Liu, C.-C. Chu, "Wide-area measurement-based voltage stability indicators by modified coupled single-port models," *IEEE Trans. Power Systems*, vol. 29, no. 2, pp. 756-764, 2014.

[18] W. Xu, et al., "A network decoupling transform for phasor data based voltage stability analysis and monitoring," *IEEE Trans. Smart Grid*, vol. 3, no. 1, pp. 261–270, Mar.2012.

[19] I. R. Pordanjani, et al, "Identification of critical components for voltage stability assessment using channel components transform," *IEEE Trans. Smart Grid*, vol. 4, no. 2, pp. 1122-1132, 2013.

[20] P. Zhang, L. Min, J. Chen, Measurement-based voltage stability monitoring and control, *US Patent 8,126,667*, 2012

[21] K. Sun, P. Zhang, L. Min, Measurement-based voltage stability monitoring and control for load centers, *EPRI Report No. 1017798*, 2009.

[22] F. Galvan, A. Abur, K. Sun et al., "Implementation of synchrophasor monitoring at Entergy: Tools, training and tribulations." *IEEE PES General Meeting*, 2012.

[23] K. Sun, F. Hu, N. Bhatt, "A new approach for real-time voltage stability monitoring using PMUs." *2014 IEEE ISGT - Asia*, Kuala Lumpur, 20-23 May 2014

[24] H. Yuan, F. Li, "Hybrid voltage stability assessment (VSA) for N-1 contingency," *Electric Power Systems Research*, vol. 122, pp. 65–75, May. 2015.
[25] F. Hu, K. Sun, et al, "An adaptive three-bus power system equivalent for estimating voltage stability margin from synchronized phasor measurements," *IEEE PES General Meeting*, 2014.
[26] J. Nocedal, and S. J. Wright, "Numerical Optimization 2nd," 2006.
[27] J. H. Chow, R. Galarza, P. Accari et al., "Inertial and slow coherency aggregation algorithms for power system dynamic model reduction," *IEEE Trans. Power Systems*, vol. 10, no. 2, pp. 680-685, 1995

IX. BIOGRAPHIES

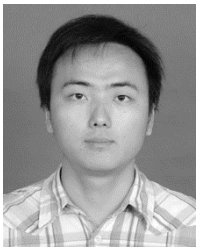

Fengkai Hu (S'14) received the B.S. and M.S. degrees in automation from University of Electronic Science and Technology of China, Chengdu, China, in 2009 and 2012, respectively. He is currently working toward the Ph.D. degree in electrical engineering in the University of Tennessee, Knoxville, TN, USA. His research interests include voltage stability and control, wide area measurement system visualization and smart grid communication.

Kai Sun (M'06–SM'13) received the B.S. degree in automation in 1999 and the Ph.D. degree in control science and engineering in 2004 both from Tsinghua University, Beijing, China. He was a postdoctoral research associate at Arizona State University, Tempe, from 2005 to 2007, and was a project manager in grid operations and planning areas at EPRI, Palo Alto, CA from 2007 to 2012.

He is currently an assistant professor at the Department of EECS, University of Tennessee in Knoxville. His research interests include power system dynamics, stability and control and complex systems.

Alberto Del Rosso (M'07) received his PhD degree from the Instituto de Energía Eléctrica, in Argentina, and Electromechanical Engineer diploma from the Universidad Tecnológica Nacional (UTN), Mendoza-Argentina. He was visiting researcher at the Department of Electrical & Computer Engineer of the University of Waterloo in Ontario Canada.

Dr. Del Rosso is currently with EPRI, Knoxville, TN. He leads the EPRI's Transmission Modernization Demonstration (TMD) Initiative, and has also managed a variety of R&D and engineering projects related with transmission planning, smart grid technologies, transmission system operation optimization, dynamic security assessment, reactive power planning, wind generation integration, and vulnerability of nuclear power plants, among others. Formerly he worked for many years as power system consultant. He chairs and actively participates in several task forces and working groups at the CIGRE, IEEE and NERC.

Evangelos Farantatos (S'06, M '13) was born in Athens, Greece in 1983. He received the Diploma in Electrical and Computer Engineering from the National Technical University of Athens, Greece, in 2006 and the M.S. in E.C.E. and Ph.D. degrees from the Georgia Institute of Technology in 2009 and 2012 respectively. He is currently a Sr. Project Engineer/Scientist at EPRI. In summer 2009, he was an intern in MISO. His research interests include power systems state estimation, protection, stability, operation, control, synchrophasor applications, renewables integration and smart grid technologies.

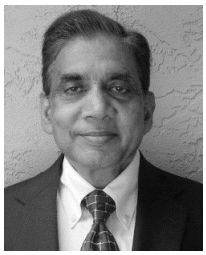

Navin B. Bhatt (F'09) received a BSEE degree from India, and MSEE and PhD degrees in electric power engineering from the West Virginia University, Morgantown, WV, USA. He works at EPRI since July 2010, where his activities focus on R&D in the smart transmission grid, and transmission operations & planning areas. Before joining EPRI, Dr. Bhatt worked at AEP for 33 years, where he conducted, managed and directed activities related to advanced analytical studies; managed AEP's transmission R&D program; participated in the development of NERC standards; and participated in North American Synchrophasor Initiative (NASPI) activities.

Dr. Bhatt is a licensed Professional Engineer in Ohio. He has authored/co-authored over 50 technical papers. Dr. Bhatt was a member of the NERC technical team that investigated the August 14, 2003 blackout on behalf of the US and Canadian governments. He was a co-author of an IEEE working group paper that received in 2009 an award as an Outstanding Technical Paper. Dr. Bhatt has chaired 3 NERC teams and a NASPI task team.